Appendix 3: Input, Calibration, Uncertainty, and Limitations of the Basin Characterization Model

By Alan L. Flint, Lorraine E. Flint, and Melissa D. Masbruch

Appendix 3 of
Conceptual Model of the Great Basin Carbonate and Alluvial Aquifer System

Edited by Victor M. Heilweil and Lynette E. Brooks

Scientific Investigations Report 2010–5193

U.S. Department of the Interior
U.S. Geological Survey

U.S. Department of the Interior
KEN SALAZAR, Secretary

U.S. Geological Survey
Marcia K. McNutt, Director

U.S. Geological Survey, Reston, Virginia: 2011

Suggested citation:
Heilweil, V.M., and Brooks, L.E., eds., 2011, Conceptual model of the Great Basin carbonate and alluvial aquifer system: U.S. Geological Survey Scientific Investigations Report 2010-5193, 188 p.

Contents

Figures

Tables

Conversion Factors

Inch/Pound to SI

Multiply	By	To obtain
	Length	
inch (in.)	2.54	centimeter (cm)
inch (in.)	25.4	millimeter (mm)
foot (ft)	0.3048	meter (m)
mile (mi)	1.609	kilometer (km)
	Area	
acre	4,047	square meter (m^2)
acre	0.4047	hectare (ha)
square mile (mi^2)	2.590	square kilometer (km^2)
	Volume	
gallon (gal)	3.785	liter (L)
gallon (gal)	0.003785	cubic meter (m^3)
gallon (gal)	3.785	cubic decimeter (dm^3)
cubic foot (ft^3)	28.32	cubic decimeter (dm^3)
cubic foot (ft^3)	0.02832	cubic meter (m^3)
acre-foot (acre-ft)	1,233	cubic meter (m^3)
acre-foot (acre-ft)	0.001233	cubic hectometer (hm^3)
	Flow rate	
acre-foot per year (acre-ft/yr)	1,233	cubic meter per year (m^3/yr)
acre-foot per year (acre-ft/yr)	0.001233	cubic hectometer per year (hm^3/yr)
foot per year (ft/yr)	0.3048	meter per year (m/yr)
cubic foot per second (ft^3/s)	0.02832	cubic meter per second (m^3/s)
cubic foot per day (ft^3/d)	0.02832	cubic meter per day (m^3/d)
gallon per minute (gal/min)	0.06309	liter per second (L/s)
	Hydraulic conductivity	
foot per day (ft/d)	0.3048	meter per day (m/d)
inch per day (in./d)	25.38	millimeter per day (mm/d)
	Transmissivity*	
foot squared per day (ft^2/d)	0.09290	meter squared per day (m^2/d)

Note: The conversion factors given above are for the entire report. Not all listed conversion factors will be in any given chapter of this report.

Temperature in degrees Celsius (°C) may be converted to degrees Fahrenheit (°F) as follows:
°F=(1.8×°C)+32

Temperature in degrees Fahrenheit (°F) may be converted to degrees Celsius (°C) as follows:
°C=(°F-32)/1.8

Temperature in kelvin (K) may be converted to degrees Fahrenheit (°F) as follows:
°F=1.8K-459.67

Temperature in kelvin (K) may be converted to degrees Celsius (°C) as follows:
°C=K-273.15

Vertical coordinate information is referenced to the North American Vertical Datum of 1988 (NAVD 88).

Horizontal coordinate information is referenced to the North American Datum of 1983 (NAD 83).

Altitude, as used in this report, refers to distance above the vertical datum.

*Transmissivity: The standard unit for transmissivity is cubic foot per day per square foot times foot of aquifer thickness [(ft^3/d)/ft^2]ft. In this report, the mathematically reduced form, foot squared per day (ft^2/d), is used for convenience.

Appendix 3: Input, Calibration, Uncertainty, and Limitations of the Basin Characterization Model

By Alan L. Flint, Lorraine E. Flint, and Melissa D. Masbruch

An overview of the Basin Characterization Model (BCM) is given in the main text of this report and in Flint, A.L., and Flint, L.E. (2007). Briefly, BCM is a quasi-physical model that simulates the surface-water balance accounting for precipitation, snow accumulation and melt, evapotranspiration, soil moisture, storage, movement, and bedrock saturated hydraulic conductivity to calculate the potential runoff and potential in-place recharge. The model requires spatially distributed data to quantify and simulate each component of the surface-water balance. The flow chart shown in figure A3–1 illustrates the major model components and the relations between components. The following sections describe the input files, model uncertainty, model limitations, and instructions for running the BCM.

Spatially Distributed Input Data

Large scale digital data sets were compiled for the major water-budget components and processes. The sources, resolutions, data components used, and additional processing done on the datasets are described in this section. A digital elevation model (DEM), available as a 30-m resolution DEM (Elevation Derivatives for National Applications, EDNA; http://edna.usgs.gov), was resampled to a 270-m resolution grid. Finer resolution grid dimensions were tested, but required too much computational time for the BCM runs. This grid provides the spatial resolution and extent for the development of all input files that are used to simulate available water for recharge.

Soil properties were extracted from soil maps obtained from the State Soil Geographic Database (STATSGO; http://www.ftw.nrcs.usda.gov/stat_data.html), a state-compiled geospatial database of soil properties that generally are consistent across state boundaries (Soil Conservation Service, 1991). The soil maps for STATSGO are compiled by generalizing more detailed soil survey maps. Mapped soil types are identified in the STATSGO database using a unique map unit identifier (MUID), representing groups of similar soil types. Although the location of a given soil component within a mapped MUID area is not known, the percentage of MUID area covered by each component is defined, and the maximum and minimum thickness of all layers in each component is provided. The database provides soil attributes for each MUID, including porosity, thickness, and percentages of particle sizes for sand, silt, and clay. Soil attributes associated with each MUID were averaged using the combined weight of layer thickness and area for the soil components in each MUID. Soil thickness was obtained directly from STATSGO data for all locations other than where Quaternary basin fill (alluvium) was mapped on geology maps. In locations with alluvium, a total depth of 6 m was chosen on the basis of field observations made in the Mojave Desert of desert plant root penetration into alluvium and bedrock. This assumes that all processes controlling net infiltration occur within the top 6 m of the surficial materials, as shown by Flint and Flint (1995) for Yucca Mountain in the southern Great Basin, and that any water penetrating below 6 m in deep alluvium is recharge. Total soil-water storage capacity was calculated by multiplying soil thickness by soil porosity (Topp and Ferre, 2002). Soil water content at field capacity (-0.01 megapascals (MPa)) and plant wilting point (-6 MPa) were calculated using the average percentage of sand and clay for each MUID and empirical equations from Campbell (1985).

The surficial geologic unit identification is classified broadly for the purpose of assigning saturated hydraulic conductivity values to consolidated surficial bedrock and unconsolidated deposits throughout the region (table A3–1). These geologic units were obtained from geologic maps for each state (California: Jennings, 1977; Idaho: Johnson and Raines, 1996; Nevada: Stewart and others, 2003; Utah: Hintze and others, 2000). The principal geologic units include Quaternary to Tertiary unconsolidated to slightly indurated alluvial, eolian, playa and lacustrine deposits, and volcanic rocks; Mesozoic granitic and other intrusive rocks, sandstone, limestone, and other metasediments, metavolcanic and metamorphic rocks; Paleozoic carbonate and clastic rocks (quartzite, argillite, shale); and Precambrian clastic sedimentary and metamorphic rocks. The surficial geologic units were generalized on the basis of saturated hydraulic conductivity rather than geologic age. The saturated hydraulic conductivity was estimated for each surficial bedrock or unconsolidated surficial unit. Initial saturated hydraulic conductivities were estimated from literature, aquifer-test results, surface-based infiltration experiments, and expert

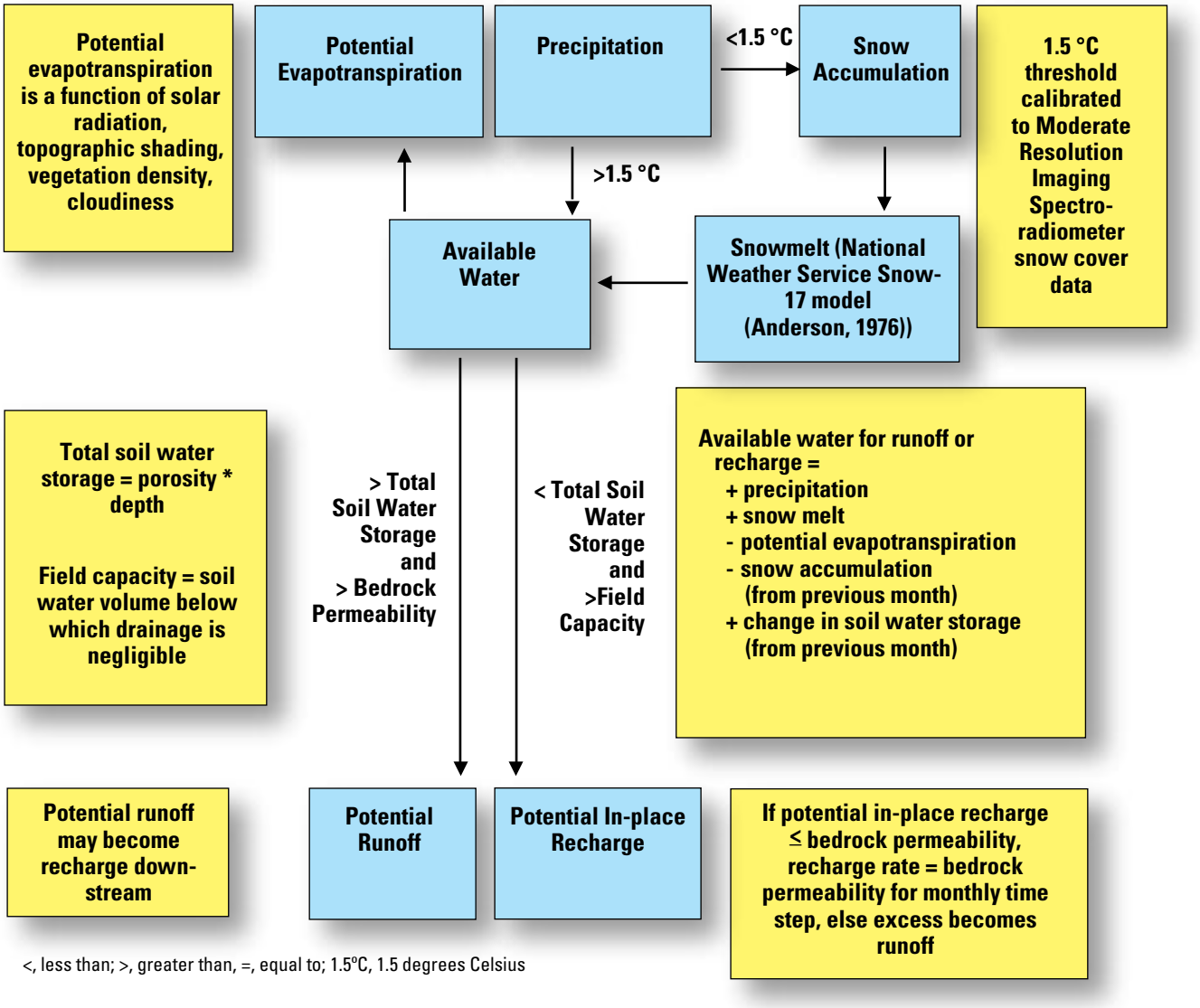

Figure A3–1. Relation of components of the Basin Characterization Model used to calculate potential runoff and in-place recharge at a monthly time step.

opinion from field geologists, and refined during calibration whereby basin runoff estimates were matched to measured streamflow (see "Calibration of Input Data" below). The hydraulic properties of macropores and fractures are incorporated in the bulk estimates of hydraulic conductivity. Hydraulic conductivity estimates of bedrock vary over several orders of magnitude and are uncertain because of the unknown hydraulic properties and spatial distributions of fractures, faults, fault gouge, and shallow infilling materials associated with different bedrock types.

Quaternary basin-fill deposits have the highest saturated hydraulic conductivity in the study area, particularly the eolian deposits and sand and gravel units, whereas finer grained flood-plain deposits, clay-rich lacustrine deposits, and playa deposits generally have the lowest saturated hydraulic conductivity values of the basin-fill deposits. Saturated hydraulic conductivity of surficial bedrock is not equivalent to transmissivity due to surface weathering and infilling of fractures and faults from soils and calcium carbonate development. However, relative estimates among rock types can be derived on the basis of groundwater assessments. Carbonates and sandstones are generally the most permeable of the consolidated rocks (Bedinger and others, 1989), and where fractured and porous have similar permeabilities as the sand and gravel aquifers in the basin fill (Winograd and Thordarson, 1975; Dettinger and others, 2000). Granitic rocks, metamorphic rocks (slates, argillites, marbles, and quartzites), and fine-grained sedimentary rocks (siltstones and shales) typically have very low permeabilities and porosities (Davis and DeWiest, 1966; Freeze and Cherry, 1979). Basalt flows and welded tuffs can be highly permeable and have sufficient porosity to store and transmit large quantities of water

Table A3–1. Surficial bedrock saturated hydraulic conductivity for different geologic units used in the Basin Characterization Model.

[Saturated hydraulic conductivity: ft/d, feet per day, rounded to two significant figures. Abbreviations: ID, identification]

Geologic unit ID	Geologic unit name	Saturated hydraulic conductivity (ft/d)	Percentage of study area
1	Basin fill—ash	1.1E+01	0.000
2	Basin fill—channels	1.1E+01	0.013
3	Basin fill—eolian sand	1.3E+01	0.600
4	Basin fill—glacial till	6.6E-02	0.168
5	Alluvium—gravels	4.5E+00	0.355
6	Alluvium—lake sediments	8.9E-04	8.112
7	Alluvium—landslides	8.2E+00	0.060
8	Alluvium—marshes	1.8E-01	0.522
9	Alluvium—mud and salt flats	9.0E-03	5.770
10	Alluvium—older upland soils	9.0E-01	3.291
11	Alluvium—playas	2.7E-03	1.559
12	Alluvium—valley fill	4.5E+00	38.071
13	Carbonates—dolomite	2.0E-01	2.624
14	Carbonates—Kaibab limestone	2.6E+00	0.287
15	Carbonates—limestone	3.3E-02	6.240
16	Carbonates—travertine	8.9E-04	0.000
17	Chert	3.3E-04	0.558
18	Conglomerate	3.3E-03	4.555
19	Gabbro	8.9E-04	0.000
20	Granite	4.9E-03	1.031
21	Granite—granodiorite	2.0E-02	0.006
22	Granite—mixed	1.6E-03	0.007
23	Granite—quartz monzonite	1.3E-02	0.702
24	Igneous—diabase	9.0E-02	0.027
25	Igneous—dikes and plugs	8.9E-04	0.001
26	Metamorphics—gneiss/schist	1.6E-03	0.862
27	Metamorphics—phyllite	6.6E-03	0.128
28	Metamorphics—serpentinite	3.3E-03	0.001
29	Metasediments	3.3E-02	0.017
30	Metavolcanics	3.3E-04	0.025
31	Quartzite	1.6E-04	1.016
32	Sandstone	1.6E-02	0.483
33	Sandstone—Brushy Basin	9.0E-03	0.004
34	Sandstone—Castle Valle	3.3E-02	0.167
35	Sandstone—Chinle	9.0E-03	0.000
36	Sandstone—Cliff House	2.7E-01	0.000
37	Sandstone—Coconino	1.6E-01	0.000
38	Sandstone—Crazy Hollow	2.7E-01	0.088
39	Sandstone—Dakota	2.7E-01	0.000
40	Sandstone—Moenkopi	4.5E-03	0.150
41	Sandstone—Navajo	1.6E+00	0.595
42	Sandstone—claystone	4.5E-03	0.031
43	Sandstone—fine	3.3E-03	0.795
44	Sandstone—shale	3.3E-04	2.879
45	Sandstone—siltstone	4.5E-03	0.817
46	Sedimentary—shale/limestone	3.3E-01	0.441
47	Sedimentary	4.5E-02	0.000
48	Volcanics—andesites	8.9E-04	0.004
49	Volcanics—andesites (flows and breccias)	1.6E-02	1.366
50	Volcanics—ash-flow tuffs, undifferentiated	6.6E-03	7.750
51	Volcanics—ash-flow tuffs, welded	1.6E-03	1.472
52	Volcanics—ash-flow tuffs, nonwelded	1.6E-02	0.022
53	Volcanics—basalts	2.6E-04	0.392
54	Volcanics—breccias	8.9E-04	0.037
55	Volcanics—lava flows	4.9E-02	3.329
56	Volcanics—pyroclastics	3.3E-03	2.569
57	Volcanics—rhyolites	3.3E-04	0.000

(Glancy, 1986; Winograd and Thordarson, 1975). Typically, volcanic rocks in the desert Southwest are far less porous and permeable than the sand and gravel of the basin fill or the carbonate rocks.

The primary geologic unit exposed at the surface of the GBCAAS study area is alluvium (valley fill), having an estimated saturated hydraulic conductivity of 4.5 ft/d and covering about 38 percent of the study area (table A3–1). Carbonates comprise the second most abundant surficial geologic unit, including both limestone (0.033 ft/d; about 6 percent of study area) and dolomite (0.2 ft/d; about 3 percent of study area). Next are volcanic rocks, including both undifferentiated ash-flow tuffs (0.0066 ft/d; about 8 percent) and welded ash-flow tuffs (0.0016 ft/d; about 1 percent). Other substantial surficial geologic units include alluvium (lake sediments) (0.00089 ft/d; about 8 percent), alluvium (mud and salt flats) (0.009 ft/d; about 6 percent), and conglomerate (0.0033 ft/d, about 5 percent).

Estimated saturated hydraulic-conductivity values used in the BCM range from about 0.00016 ft/d for quartzite to about 13 ft/d for basin fill (eolian sand), but these extremes occur at the surface in only small portions of the GBCAAS study area (table A3–1). Eolian sand covers about 0.6 percent of the study area, primarily in the Great Salt Lake Desert (37) and Sevier Lake (39) groundwater flow systems (fig. B–3). In addition to eolian sand, the highest permeability geologic units include basin-fill ash and channel deposits, both having an estimated hydraulic conductivity of 11 ft/d (table A3–1). The highest hydraulic conductivity values for consolidated rock include the Navajo Sandstone (1.6 ft/d) and the Kaibab

Limestone (2.6 ft/d). The Navajo and Kaibab outcrops in about 6 and 2 percent of the study area, respectively. Both of these permeable bedrock formations are located predominantly in the Great Salt Lake Desert (37), Great Salt Lake (38), and Sevier Lake (39) groundwater flow systems. Low-permeability quartzite outcrops in about 1 percent of the GBCAAS study area. Other low-permeability geologic units include alluvium (lake sediments) (0.00089 ft/d) and shale (0.00033 ft/d), covering about 8 and 3 percent of study area, respectively. These low-permeability formations are primarily located in the Great Salt Lake (38), Great Salt Lake Desert (37), and Sevier Lake (39) groundwater flow systems. Nine of the 57 geologic units in table A3–1 are not present within the GBCAAS study area, but are included in the table, which was generated for the larger areal extent of the BCM model in the western United States.

Temporally Distributed Input Data

Spatially distributed monthly estimates of precipitation, minimum and maximum air temperature, and potential evapotranspiration were used to calculate a surface-water budget and to partition the water available for runoff and in-place recharge on the basis of the spatially distributed estimates of soil-water storage capacity and saturated hydraulic conductivity of the underlying consolidated rock and basin-fill deposits. Locations and quantities of excess water were estimated on a monthly basis. Spatially distributed estimates of monthly precipitation and maximum and minimum monthly air temperatures were approximated using monthly climate data from 1940 to 2006, available at 4,000-m grid spacing (Daly and others, 2008; available from http://www.prism.oregonstate.edu/products/matrix.phtml). The centroids of the grids were used in the downscaling of the data to the 270-m grid by applying a model from Nalder and Wein (1998) that combines a spatial gradient plus inverse-distance squared weighting (GIDS) using multiple regression with northing, easting, and elevation (Flint, L.E., and Flint, A.L, 2007). The long-term record was used in a transient analysis that is conducted to include the effects of antecedent soil moisture and, thus, better reflect the impact of historical climatic trends on hydrologic response.

For this study the Priestley-Taylor equation was used to estimate potential evapotranspiration (PET; Priestley and Taylor, 1972):

$$PET = \alpha \bullet s / (s + \gamma) \bullet (Rn - G) / \lambda \qquad \text{(A1–1)}$$

where

- α is the Priestley-Taylor coefficient and is set to 1.26,
- s is the slope of the vapor deficit curve,
- γ is the psychometric constant,
- Rn is net radiation,
- G is soil heat flux, and
- λ is the latent heat of vaporization.

G is calculated from monthly air temperature using the method of Shuttleworth (1993, equation 4.2.17) and Rn is calculated using the radiation balance equation:

$$Rn = K\downarrow \bullet (1 - a) + L\downarrow + L\uparrow \qquad \text{(A1–2)}$$

where

- $K\downarrow$ is incoming solar radiation, a is surface albedo,
- $L\downarrow$ is incoming long wave radiation, and
- $L\uparrow$ is outgoing long wave radiation.

Incoming solar radiation ($K\downarrow$) is the main energy source for evapotranspiration but it can be reduced or enhanced by the slope and aspect of the site being modeled relative to the sun's elevation and azimuth, determined on an hourly basis. In addition, the solar radiation can be greatly reduced in mountainous terrain by topographic shading (determined by the sun's elevation and azimuth and the elevation of the surrounding topography that will block the sun during the day) (Flint and Childs, 1987). Solar radiation is reduced by atmospheric water vapor, ozone, aerosols, and air molecules, which are accounted for in the solar radiation model of Flint and Childs (1987) and used in this study. Clouds also reduce incoming solar radiation and are estimated for average months using the National Radiation Energy Laboratory (NREL) database from 1960 to 1990 (http://rredc.nrel.gov/solar/old_data/nsrdb/1961-1990/). Albedo (a) is varied monthly and distributed spatially using an inverse-distance squared method and data from Iqbal (1983). Incoming and outgoing long wave radiation (L↓ and L↑) are determined using the Stefan-Boltzmann radiative emission equation:

$$L\downarrow \text{ or } L\uparrow = \varepsilon \sigma T^4 \qquad \text{(A1–3)}$$

where

- T is air temperature (for L↓) or surface temperature (for L↑), in degrees Kelvin;
- σ is the Stefan-Boltzmann constant; and
- ε is atmospheric emissivity for clear sky for calculating (L↓) and was determined using the equation of Swinbank (1963).

$$\varepsilon = 0.0000092\ T^2 \qquad \text{(A1–4)}$$

where

- T is air temperature for outgoing long wave radiation (L↑), in degrees Kelvin; and
- ε is surface emissivity assumed to be 0.98 for all surfaces.

Clouds have an emissivity of 1, so ε will range from the value calculated by Swinbank (1963) for clear sky to a value of 1 for full cloudy sky, and is proportional between clear sky emissivity and full cloudy sky emissivity based on the percent of clouds. This approach uses the monthly average cloudiness from the NREL cloudiness data base discussed above. Evapotranspiration is assumed to occur at the potential rate until there is no additional water available (the soil reaches wilting point), at which point it is zero.

Soil Water Accounting

Where soils are present, soil thickness, porosity, drainage characteristics, and antecedent (previous month) soil moisture determine how much precipitation and snowmelt is added into the soil zone. If the new calculated soil water content exceeds soil water storage, excess water is allowed to infiltrate into the underlying material at a rate equal to the saturated hydraulic conductivity of the underlying material, assuming a unit vertical hydraulic gradient. If the saturated hydraulic conductivity (ft/day) of the underlying material is less than the excess water (ft) for the month (for the number of days in the month), then the maximum infiltration is calculated as in-place recharge and the excess is calculated as runoff for that month. If the new calculated soil water content does not exceed soil-water storage capacity, but does exceed field capacity, then excess water is allowed to infiltrate at a rate equal to the saturated hydraulic conductivity of the underlying material, with any remaining water allowed to stay in the soil profile until the following month.

Calibration of the Basin Characterization Model

BCM input data and the final BCM results are calibrated or verified in various steps. The solar radiation calculations in the submodel for potential evapotranspiration compared very well to measured average monthly cloud-free data from the Natural Renewable Energy Laboratory for 1960–1990 (http://rredc.nrel.gov/solar/old_data/nsrdb/1961-1990/) and corrections were then added to the submodel to correlate with the average monthly cloudiness data. The resultant potential evapotranspiration was compared with ETo, the calculation for reference crop evapotranspiration, calculated from measured data for the state of California (http://wwwcimis.water.ca.gov/cimis/) and the state of Arizona (http://ag.arizona.edu/azmet/). Simulated monthly potential evapotranspiration using the BCM compares well to monthly ETo from these networks, with slight overestimates in June, July, and August on the order of approximately 10 percent. No ETo data was available for Utah or Nevada, however, estimates of potential evaporation calculated from meteorological data in Nevada compared well with the BCM (Flint and others, 2008), suggesting the detailed calibration in California and Arizona were adequate for the study area.

BCM snow accumulation and snowmelt were compared to Moderate Resolution Imaging Spectroradiometer (MODIS) snowcover remotely sensed data (https://lpdaac.usgs.gov/lpdaac/products/modis_products_table) for visual comparison of snowcover extent, and was adjusted by varying the temperature threshold at which melt occurs (Lundquist and Flint, 2006). Energy and mass balance calculations for snow accumulation and ablation were adapted by Lundquist and Flint (2006) from the operational Snow–17 model (Anderson, 1976; Shamir and Georgakakos, 2005) of the National Weather Service (NWS). Snow–17 is a snowpack energy balance model that uses minimum, maximum, and average air temperature (changing at 6 hour intervals) and an empirical melt factor that varies with day of year to increase or decrease the heat deficit in the snowpack. Once it rises above 0ºC degrees Celsius, snow can melt. The adapted Snow–17 model is applied to every model grid cell so that the spatial distribution, as well as snow water equivalent, is calculated over the modeling domain at each time step. Calibration was performed by varying the air temperature threshold below which precipitation was in the form of snow; this was determined to be 1.5ºC. Sublimation of snow was calculated as a standard rate (5 mm/month), and snowmelt was based on the snowpack energy balance when air temperatures were above freezing. Although snow distribution at maximum snowpack is over- and underestimated to some degree, the calculation of snowmelt reasonably represents snowmelt during the predominant period of runoff. Examples of measured and predicted snowcover for maximum accumulation and snowmelt periods are illustrated in Flint and Flint (2007).

Runoff calibration and recharge calculation by the BCM were done by changing the bedrock saturated hydraulic conductivity values used for the various geologic units. The bedrock saturated hydraulic conductivity values were modified by optimizing the match between modeled runoff and estimated runoff from streamflow records of 67 gages located in 44 hydrographic areas within the study area that have distinct surficial bedrock geology (table A3–2). Estimated runoff was determined by subtracting baseflow (mean annual minimum discharge for period of record) from the total discharge (mean discharge for the period of record) for each gage. Optimizing saturated hydraulic conductivity for each of the geologic units was difficult because: (1) each watershed used in the calibration contained mixed geology, and, thus, the runoff-producing geologic unit listed in table A3–2 was not necessarily the dominant surficial geologic unit within the watershed; instead it was generally the lowest permeability rock type found in the highest precipitation zone (highest altitude); and (or) (2) a geologic unit may occur in more than one watershed used for the calibration, however, the hydraulic conductivity for each geologic unit had to be consistent across the GBCAAS study area. For example, increasing the bedrock permeability from 0.1 to 1 mm/day for volcanic rhyolites results in reductions in simulated BCM runoff of between 170 and 260 percent for four watersheds near Beaver, Utah (Three Creeks, Beaver River, South Creek, and North Fork North Creek). The reduced BCM runoff more closely matched estimated runoff at three stream gages, whereas the reduced BCM runoff was too low for Beaver River. This illustrates the complexity of calibrating the BCM to streamflow measurements when using regional geology maps with multiple geologic units of varying percentages in different basins.

Table A3–2. Comparison of estimated runoff from streamflow records to BCM runoff used for calibration of surficial bedrock saturated hydraulic conductivity.

[Site number, U.S. Geological Survey gaging site number. Latitude and Longitude: in decimal degrees, datum NAD83. Mean annual discharge: for period of record. Baseflow: mean annual minimum discharge for period of record. Estimated runoff: calculated as the difference between mean annual discharge and baseflow. BCM as percent of estimated runoff: BCM runoff divided by estimated runoff. Abbreviations: ID, identification; ft, feet; acre-ft/yr, acre-feet per year]

Stream gage station number	Station name	Hydrographic area number	Dominant runoff-producing geologic unit ID	Dominant runoff-producing geologic unit name
10104700	Little Bear River below Davenport Creek near Avon, Utah	272	12	Alluvium—valley fill
10102300	Summit Creek above diversions near Smithfield, Utah	272	13	Carbonates—dolomite
10109000 and 10108400	Combined flow of Logan River above State Dam and Logan, Hyde Park & Smithfield Canal at head, near Logan, Utah	272	13	Carbonates—dolomite
10145000	Mill Creek at Mueller Park near Bountiful, Utah	268	15	Carbonates—limestone
10166430	West Canyon Creek near Cedar Fort, Utah	264	15	Carbonates—limestone
10172791	Settlement Creek above reservoir near Tooele, Utah	262	15	Carbonates—limestone
10251890	Peak Spring Canyon Creek near Charleston Peak, Nevada	162	15	Carbonates—limestone
10249280	Kingston Creek below Cougar Canyon near Austin, Nevada	137B	17	Chert
10317400	North Fork Humboldt River near North Fork, Nevada	44	17	Chert
10146000	Salt Creek at Nephi, Utah	266	18	Conglomerate
10148400	Nebo Creek near Thistle, Utah	265	18	Conglomerate
10148500	Spanish Fork at Thistle, Utah	265	18	Conglomerate
10219200	Chicken Creek near Levan, Utah	285	18	Conglomerate
10233000	Meadow Creek near Meadow, Utah	286	18	Conglomerate
10233500	Corn Creek near Kanosh, Utah	286	18	Conglomerate
10244720	Franklin River near Arthur, Nevada	176	20	Granite
10244745	Overland Creek near Ruby Valley, Nevada	176	20	Granite
10316500	Lamoille Creek near Lamoille, Nevada	45	20	Granite
10141500	Holmes Creek near Kaysville, Utah	268	26	Metamorphics—gneiss/schist
10142000	Farmington Creek above diversions near Farmington, Utah	268	26	Metamorphics—gneiss/schist
10142500	Ricks Creek above diversions near Centerville, Utah	268	26	Metamorphics—gneiss/schist
10143000	Parrish Creek above diversions near Centerville, Utah	268	26	Metamorphics—gneiss/schist
10143500	Centerville Creek above diversions near Centerville, Utah	268	26	Metamorphics—gneiss/schist
10144000	Stone Creek above diversions near Bountiful, Utah	268	26	Metamorphics—gneiss/schist
10164500	American Fork above Upper Powerplant near American Fork, Utah	265	26	Metamorphics—gneiss/schist
10168500	Big Cottonwood Creek near Salt Lake City, Utah	267	26	Metamorphics—gneiss/schist
10172700	Vernon Creek near Vernon, Utah	263	26	Metamorphics—gneiss/schist
10172870	Trout Creek near Callao, Utah	254	26	Metamorphics—gneiss/schist
10172952	Dunn Creek near Park Valley, Utah	260B	26	Metamorphics—gneiss/schist
10224100	Oak Creek above Little Creek near Oak City, Utah	287	26	Metamorphics—gneiss/schist
10172800	South Willow Creek near Grantsville, Utah	262	31	Quartzite
10172805	North Willow Creek near Grantsville, Utah	262	31	Quartzite
10243240	Baker Creek at Narrows near Baker, Nevada	254	31	Quartzite
10104900	East Fork Little Bear River above reservoir near Avon, Utah	272	43	Sandstone—fine
10105000	East Fork Little Bear River near Avon, Utah	272	43	Sandstone—fine
10148200	Tie Fork near Soldier Summit, Utah	265	43	Sandstone—fine
10242000	Coal Creek near Cedar City, Utah	282	43	Sandstone—fine
9415515	Water Canyon Creek near Preston, Nevada	207	44	Sandstone—shale
10099000	High Creek near Richmond, Utah	272	44	Sandstone—shale
10111700	Blacksmith Fork below Mill Creek near Hyrum, Utah	272	44	Sandstone—shale
10113500	Blacksmith Fork above Utah Power & Light Company's Dam, near Hyrum, Utah	272	44	Sandstone—shale

Table A3–2. Comparison of estimated runoff from streamflow records to BCM runoff used for calibration of surficial bedrock saturated hydraulic conductivity.—Continued

[Site number, U.S. Geological Survey gaging site number. Latitude and Longitude: in decimal degrees, datum NAD83. Mean annual discharge: for period of record. Baseflow: mean annual minimum discharge for period of record. Estimated runoff: calculated as the difference between mean annual discharge and baseflow. BCM as percent of estimated runoff: BCM runoff divided by estimated runoff. Abbreviations: ID, identification; ft, feet; acre-ft/yr, acre-feet per year]

Latitude	Longitude	Altitude (ft)	Number of years	Mean annual discharge (acre-ft/yr)	Baseflow (acre-ft/yr)	Estimated runoff (acre-ft/yr)	BCM runoff (acre-ft/yr)	BCM runoff as percentage of estimated runoff
41.512436	-111.811885	5,020	32	41,543	12,756	28,787	20,956	72.80
41.869374	-111.759110	5,371	18	14,320	2,860	11,460	9,731	84.91
41.744375	-111.784387	4,680	85	178,181	63,897	114,285	53,240	46.59
40.863834	-111.836880	5,240	18	4,660	609	4,050	3,910	96.53
40.405226	-112.100496	5,620	30	2,717	276	2,441	2,180	89.33
40.505500	-112.290502	5,380	10	2,306	435	1,870	1,905	101.85
36.244407	-115.720020	6,900	14	1,417	213	1,204	607	50.36
39.212429	-117.113422	6,480	40	6,548	2,638	3,910	4,058	103.78
41.576072	-115.914956	6,700	16	7,529	218	7,311	3,929	53.74
39.713012	-111.804376	5,280	42	17,891	3,969	13,921	8,346	59.95
39.871624	-111.570196	5,720	10	11,100	3,620	7,481	9,297	124.28
39.999400	-111.499356	5,027	58	64,502	18,682	45,820	38,686	84.43
39.552180	-111.829928	5,540	33	5,698	745	4,953	2,349	47.44
38.891354	-112.327436	5,800	10	5,055	935	4,119	3,689	89.54
38.774134	-112.399659	5,300	10	12,878	3,482	9,396	9,923	105.61
40.821394	-115.135461	6,567	19	8,246	865	7,380	6,571	89.03
40.458262	-115.392550	6,450	13	8,199	699	7,499	3,342	44.56
40.690761	-115.477003	6,240	70	32,638	2,504	30,134	13,388	44.43
41.054944	-111.895218	5,095	16	2,671	986	1,684	2,554	151.64
41.001333	-111.873272	5,100	26	9,669	1,484	8,184	11,814	144.35
40.940223	-111.867438	4,860	16	1,608	339	1,269	2,082	164.10
40.923556	-111.864660	4,600	19	1,139	184	955	1,536	160.77
40.916334	-111.862993	4,680	38	2,149	678	1,471	2,473	168.13
40.894390	-111.845214	5,080	16	2,287	294	1,993	2,810	140.99
40.447730	-111.682147	5,950	62	40,862	8,368	32,494	27,245	83.84
40.618559	-111.781876	4,990	59	50,074	11,440	38,634	39,090	101.18
39.979391	-112.380230	6,200	48	2,712	1,543	1,168	6,051	517.98
39.744108	-113.889994	6,200	40	4,115	909	3,205	1,357	42.33
41.858530	-113.327219	6,250	32	3,936	654	3,283	1,299	39.57
39.356346	-112.232717	6,480	33	2,149	232	1,917	2,690	140.34
40.496331	-112.574403	6,360	43	4,842	1,767	3,076	850	27.63
40.532720	-112.572736	5,960	13	3,996	1,369	2,626	1,170	44.56
38.990780	-114.206661	6,750	15	6,578	687	5,892	6,555	111.27
41.518270	-111.714382	5,390	23	29,043	4,738	24,305	25,240	103.85
41.516603	-111.750773	5,250	12	26,306	6,498	19,809	20,717	104.58
39.949958	-111.216839	6,120	33	4,034	1,140	2,894	3,063	105.82
37.672199	-113.034670	6,000	72	24,791	4,435	20,356	20,721	101.79
38.987720	-114.958350	6,400	11	1,413	532	881	839	95.26
41.977705	-111.745222	5,250	18	24,324	4,847	19,477	13,000	66.74
41.594382	-111.567433	5,545	11	42,586	32,447	10,139	22,250	219.44
41.623545	-111.738829	5,021	87	91,335	44,261	47,074	64,590	137.21

Table A3–2. Comparison of estimated runoff from streamflow records to BCM runoff used for calibration of surficial bedrock saturated hydraulic conductivity.—Continued

[Site number, U.S. Geological Survey gaging site number. Latitude and Longitude: in decimal degrees, datum NAD83. Mean annual discharge: for period of record. Baseflow: mean annual minimum discharge for period of record. Estimated runoff: calculated as the difference between mean annual discharge and baseflow. BCM as percent of estimated runoff: BCM runoff divided by estimated runoff. Abbreviations: ID, identification; ft, feet; acre-ft/yr, acre-feet per year]

Stream gage station number	Station name	Hydrographic area number	Dominant runoff-producing geologic unit ID	Dominant runoff-producing geologic unit name
10172200	Red Butte Creek at Fort Douglas near Salt lake City, Utah	267	44	Sandstone—shale
10241600	Summit Creek near Summit, Utah	281	44	Sandstone—shale
10244950	Steptoe Creek near Ely, Nevada	179	44	Sandstone—shale
10321590	Susie Creek at Carlin, Nevada	51	44	Sandstone—shale
10321950	Maggie Creek at Maggie Creek Canyon near Carlin, Nevada	51	44	Sandstone—shale
10245445	Illipah Creek near Hamilton, Nevada	174	49	Volcanics—andesites (flows and breccias)
10234000	Three Creeks near Beaver, Utah	283	50	Volcanics—ash-flow tuffs
10234500	Beaver River near Beaver, Utah	283	50	Volcanics—ash-flow tuffs
10235000	South Creek near Beaver, Utah	283	50	Volcanics—ash-flow tuffs
10317500	North Fork Humboldt River at Devils Gate near Halleck, Nevada	44	50	Volcanics—ash-flow tuffs
10147500	Payson Creek above diversion near Payson, Utah	265	51	Volcanics—ash-flow tuffs, welded
10245900	Pine Creek near Belmont, Nevada	140B	51	Volcanics—ash-flow tuffs, welded
10245910	Mosquito Creek near Belmont, Nevada	140B	51	Volcanics—ash-flow tuffs, welded
10249300	South Twin River near Round Mountain, Nevada	137B	51	Volcanics—ash-flow tuffs, welded
10325500	Reese River near Ione, Nevada	56	51	Volcanics—ash-flow tuffs, welded
9413900	Beaver Dam Wash near Enterprise, Utah	222	52	Volcanics—ash-flow tuffs, nonwelded
9417500	Meadow Valley Wash at Eagle Canyon near Ursine, Nevada	200	52	Volcanics—ash-flow tuffs, nonwelded
10236000	North Fork North Creek near Beaver, Utah	283	52	Volcanics—ash-flow tuffs, nonwelded
10236500	South Fork North Creek near Beaver, Utah	283	52	Volcanics—ash-flow tuffs, nonwelded
10241400	Little Creek near Paragonah, Utah	281	52	Volcanics—ash-flow tuffs, nonwelded
10241430	Red Creek near Paragonah, Utah	281	52	Volcanics—ash-flow tuffs, nonwelded
10241470	Center Creek above Parowan Creek near Parowan, Utah	281	52	Volcanics—ash-flow tuffs, nonwelded
10245925	Stoneberger Creek near Austin, Nevada	140A	52	Volcanics—ash-flow tuffs, nonwelded
10246846	Lower Currant Creek near Currant, Nevada	173B	57	Volcanics—rhyolites
10246930	Sixmile Creek near Warm Springs, Nevada	156	57	Volcanics—rhyolites
10313400	Marys River below Orange Bridge near Charleston, Nevada	42	57	Volcanics—rhyolites

Table A3-2. Comparison of estimated runoff from streamflow records to BCM runoff used for calibration of surficial bedrock saturated hydraulic conductivity.—Continued

[Site number, U.S. Geological Survey gaging site number. Latitude and Longitude: in decimal degrees, datum NAD83. Mean annual discharge: for period of record. Baseflow: mean annual minimum discharge for period of record. Estimated runoff: calculated as the difference between mean annual discharge and baseflow. BCM as percent of estimated runoff: BCM runoff divided by estimated runoff. Abbreviations: ID, identification; ft, feet; acre-ft/yr, acre-feet per year]

Latitude	Longitude	Altitude (ft)	Number of years	Mean annual discharge (acre-ft/yr)	Baseflow (acre-ft/yr)	Estimated runoff (acre-ft/yr)	BCM runoff (acre-ft/yr)	BCM runoff as percentage of estimated runoff
40.779946	-111.806045	5,400	43	3,056	829	2,227	4,943	221.99
37.786921	-112.916335	6,313	23	3,412	605	2,807	3,061	109.05
39.201539	-114.689161	7,440	40	4,904	2,214	2,690	689	25.61
40.726029	-116.077855	4,910	14	7,367	12	7,355	3,245	44.11
40.803248	-116.200081	5,095	17	17,237	324	16,913	10,368	61.30
39.317764	-115.395058	6,840	11	2,446	1,400	1,046	1,242	118.78
38.294417	-112.428544	8,550	14	7,013	1,195	5,818	3,121	53.64
38.280526	-112.568271	6,200	92	37,691	10,214	27,478	14,359	52.26
38.190249	-112.552437	6,900	11	2,278	192	2,086	1,952	93.58
41.178753	-115.492575	5,370	51	54,889	3,729	51,160	45,668	89.27
39.969400	-111.693816	5,670	15	9,167	2,823	6,344	5,370	84.64
38.794376	-116.854524	7,560	28	3,977	642	3,335	3,348	100.38
38.806043	-116.679520	7,200	27	1,671	182	1,490	1,606	107.82
38.887430	-117.245367	6,400	41	5,086	811	4,275	4,895	114.51
38.857217	-117.475986	7,100	29	8,983	658	8,324	14,836	178.22
37.469975	-114.046646	4,740	15	7,345	229	7,116	6,737	94.68
38.004129	-114.206927	5,670	15	5,697	1,283	4,414	3,208	72.67
38.345527	-112.551604	6,800	11	3,930	592	3,337	2,372	71.06
38.338611	-112.537222	6,800	11	13,012	1,612	11,400	5,764	50.56
37.905530	-112.709107	6,740	21	1,378	194	1,184	177	14.91
37.856920	-112.675773	7,800	10	1,237	496	741	74	10.01
37.793032	-112.816054	6,900	23	4,763	2,358	2,405	2,259	93.94
39.140008	-116.721164	6,880	19	1,219	183	1,036	4,923	475.34
38.847159	-115.367526	6,700	24	2,405	172	2,233	869	38.92
38.573083	-116.314228	—	10	420	6	414	15	3.55
41.549913	-115.306729	5,940	15	34,820	226	34,595	27,880	80.59

Model Uncertainty

Uncertainties in BCM results pertain most significantly to uncertainties in the spatial distribution of input data such as soil type, soil thickness, soil water storage, bedrock saturated hydraulic conductivity, precipitation, and temperature. Although the estimation of bedrock saturated hydraulic conductivity introduces the most uncertainty in the final model results, it is not possible to quantify these uncertainties at a regional level. However, using changes in bedrock saturated hydraulic conductivity to calibrate the model to measured runoff reduces the total model uncertainty.

A thorough uncertainty analysis of the Parameter-elevation Regressions on Independent Slopes Model (PRISM) data used for precipitation in the BCM is available in Daly and others (2008). The authors noted that although the western mountain and desert regions are the most uncertain because of lower data density, monthly mean absolute difference in precipitation in the western U.S. on the basis of cross validation calculations comparing measured and modeled values ranged from 4.7 to 12.6 mm, and monthly air temperature ranged from 0.9 to 1.4ºC for minimum and 0.7 to 0.8ºC for maximum.

A sensitivity analysis to various input parameters was conducted for 1 year. It was determined that a year with above-average precipitation would be more appropriate than an average or below-average year because most recharge occurs during wet years. Water year 1996 was chosen because (1) it was a year of above-normal precipitation for the GBCAAS study area (fig. D–3), and (2) detailed infiltration studies during this year at Yucca Mountain were used in the initial development of the BCM (Flint and others, 2004). The parameters chosen for the sensitivity analysis were temperature, precipitation, soil thickness, and sublimation. The values selected were considered to be within the range of possible error or variation for each tested parameter: minimum and maximum monthly air temperature was increased and decreased by 3ºC; precipitation was increased and decreased by 5 percent; soil thickness was increased and decreased by 10 cm.

Limited sublimation rate data is available for the GBCAAS study area. Recently measured sublimation rates in the Sierra Nevada are as high as 15 mm/month (Alan Flint, U.S. Geological Survey, personal commun., 2009). In another study in central Idaho, sublimation rates of up to 30 mm/month have been measured (Danny Marks, U.S. Department of Agriculture, personal commun., 2009). These rates may be even higher during high wind events or during late spring as temperatures begin to warm significantly. Because sublimation is partially dependent on PET, the monthly sublimation rate for the BCM sensitivity analysis was varied by assigning a percentage of the PET rate as the sublimation rate versus the baseline simulation of using a flat rate of 5 mm/month across the entire study area. Percentages of PET tested in the sensitivity analysis ranged from 10 to 50 percent. Average monthly sublimation rates for each of the 17 groundwater flow systems using 10 percent of PET ranged from 8 to 12 mm/month; average monthly sublimation rates using 50 percent of PET ranged from 37 to 59 mm/month.

The results of the sensitivity analysis show that, for the majority of the 17 groundwater flow systems, in-place recharge is generally most sensitive to increased sublimation and increased temperature (fig. A3–2). The increase in sublimation rates to 50 percent of PET resulted in a reduced recharge of between 48 and 90 percent of the baseline simulation. Decreasing sublimation rates to 10 percent of PET resulted in an increase in recharge of between 102 and 137 percent of the baseline simulation. Increasing the monthly minimum and maximum temperature by 3ºC generally resulted in a reduced recharge of between 27 and 96 percent of the baseline simulation, except for four groundwater flow systems (Humboldt, Independence Valley, Ruby Valley, and Goshute Valley), where recharge increased to between 102 and 120 percent of baseline. Although the model was generally least sensitive to decreasing the monthly minimum and maximum temperature by 3ºC, two groundwater flow systems (Death Valley and Mesquite Valley) show substantial increases of 166 and 243 percent of baseline recharge. Decreasing the precipitation by 5 percent resulted in reduced recharge of between 72 and 94 percent of baseline. Increasing the precipitation by 5 percent resulted in an increased recharge of between 106 and 130 percent of baseline. Decreasing soil thickness by 10 cm generally resulted in an increased recharge of as much as 172 percent of baseline, while increasing soil thickness by 10 cm modified the recharge to between 44 and 102 percent of baseline. The variations shown by these sensitivity analyses reflect the uncertainties in the input data sets and the necessary simplification of physical processes for the BCM. Individual in-place recharge quantities for the 17 groundwater flow systems generally vary between 50 and 150 percent of the baseline simulation for the 1996 water year (fig. A3–2). This indicates a possible uncertainty in BCM-estimated in-place recharge of about ± 50 percent for the entire GBCAAS study area.

Another evaluation of uncertainty in the BCM in-place recharge estimates was a comparison to the estimated baseflow of 52 gaged perennial mountain streams. Because each of these streams originates within the watershed (no transbasin diversions), it is assumed this baseflow is entirely supported by in-place recharge in the same watershed. Estimated mountain-stream baseflow was calculated for each gaged stream, as described in "Discharge to Mountain Streams" (Chapter D). This analysis showed that 42 of the 52 watersheds with gaged streams had estimated baseflow that was less than or within 50 percent of BCM in-place recharge, indicating that there was sufficient BCM in-place recharge to support these perennial streams.

Mountain-stream baseflow for the remaining 10 watersheds was more than 50 percent greater than BCM in-place recharge. Most of these 10 watersheds are underlain by low permeability geologic units (metamorphic rocks and quartzite), indicating that the BCM may underestimate in-place recharge for these watersheds. These low permeability geologic units are generally fractured and the BCM may be underestimating hydraulic conductivity and overestimating runoff, resulting in insufficient in-place recharge to support

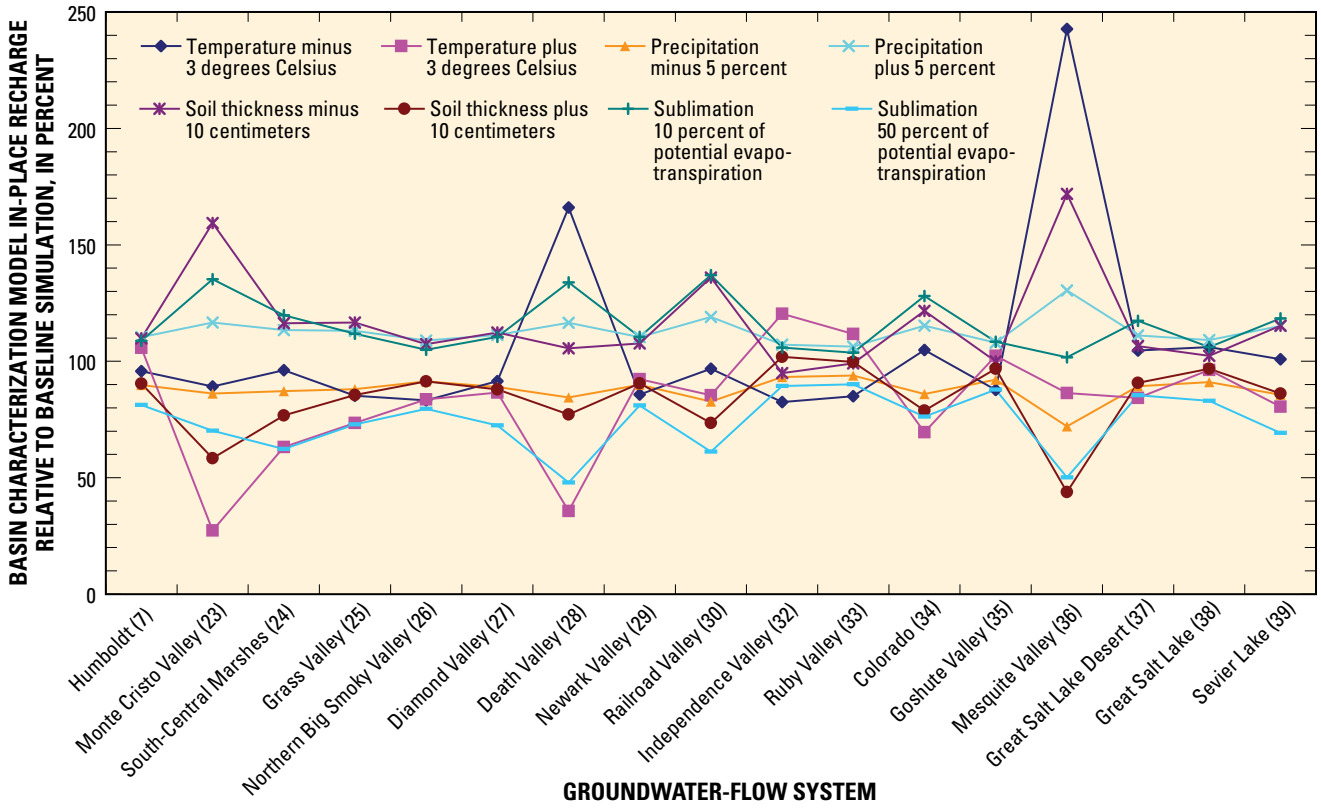

Figure A3–2. Comparison of Basin Characterization Model water year 1996 sensitivity analyses to the baseline simulation (100 percent) for the 17 groundwater flow systems within the Great Basin carbonate and alluvial aquifer system study area.

the observed mountain-stream baseflow. Another possible explanation is that the groundwater catchments for these watersheds may be larger than the surface-water catchments; therefore, the calculated volume of in-place recharge for these watersheds would have been too low.

Model Limitations

One important limitation to the BCM is that the calculation of groundwater recharge assumes that water draining past the root zone becomes recharge within that monthly time step, without consideration of the potential for extended periods of groundwater travel time in the unsaturated zone, which, in the arid and semiarid southwest may be as thick as 500 m. Calculations of groundwater travel time in the southern Great Basin have exceeded 10,000 years (Flint and others, 2000) because of low infiltration rates and unsaturated zone thicknesses exceeding 2,000 m. However, some locations in mountainous areas have shallow unsaturated zones and may recharge to local groundwater within the monthly time step. Another limitation is the use of the 1:500,000-scale geologic maps as the basis for the surficial bedrock saturated hydraulic conductivity input data. Local-scale geology is not represented in any detail at this scale and polygon areas often represent more than one rock type. This introduces error in the recharge calculations, particularly in the mountain block where the majority of in-place recharge and runoff generation occurs.

Instructions for Running the Basin Characterization Model

The BCM is run using a Fortran code, control file, and input files representing potential evapotranspiration, spatially distributed properties of soils and geologic units, and monthly files of spatially distributed climate parameters. All input files are in ASCII format and have been developed to exactly match the extent and grid size of the 270-m DEM. The BCM control file (fig. A3–3) includes input and output file names, saturated hydraulic conductivity corresponding to a surficial geologic unit identification (ID) for each of 57 bedrock geologic types, and period of time for which the model will be run. Input files are ASCII files of soil thickness, soil porosity, soil water content at wilting point and field capacity, surficial geologic unit ID, along with monthly files of precipitation, maximum and minimum air temperature, and potential evapotranspiration.

The Fortran code contains the input and output routines (I/O) to keep track of all the data for each grid cell, including snowpack and soil water storage for the preceding month. Within the Fortran code is the NWS Snow–17 model, which uses the minimum and maximum air temperature and precipitation to accumulate and melt snow that then becomes available for infiltration. Subbasins can be identified by the user and input as ASCII grid files to obtain subbasin statistics of input and output for simple analysis (that is, monthly averages of precipitation, snow, air temperature, runoff, recharge, etc.) The same values can be obtained using the monthly output ASCII grid files and zonal statistics in ArcMap or other user-written codes. Output files include monthly calculations of snow pack, snowmelt, sublimation, soil water stored, excess water (precipitation minus potential evapotranspiration), available water (precipitation minus potential evapotranspiration minus soil water storage at field capacity), potential in-place recharge (precipitation minus potential evapotranspiration minus soil water storage at field capacity plus snowmelt minus snow accumulation, and if recharge is greater than bedrock saturated hydraulic conductivity, recharge is equal to bedrock saturated hydraulic conductivity), and potential runoff (precipitation minus potential evaporation minus porosity plus snowmelt minus snow accumulation plus excess recharge if bedrock saturated hydraulic conductivity is exceeded). The potential in-place recharge and potential runoff are the two monthly files used for most applications.

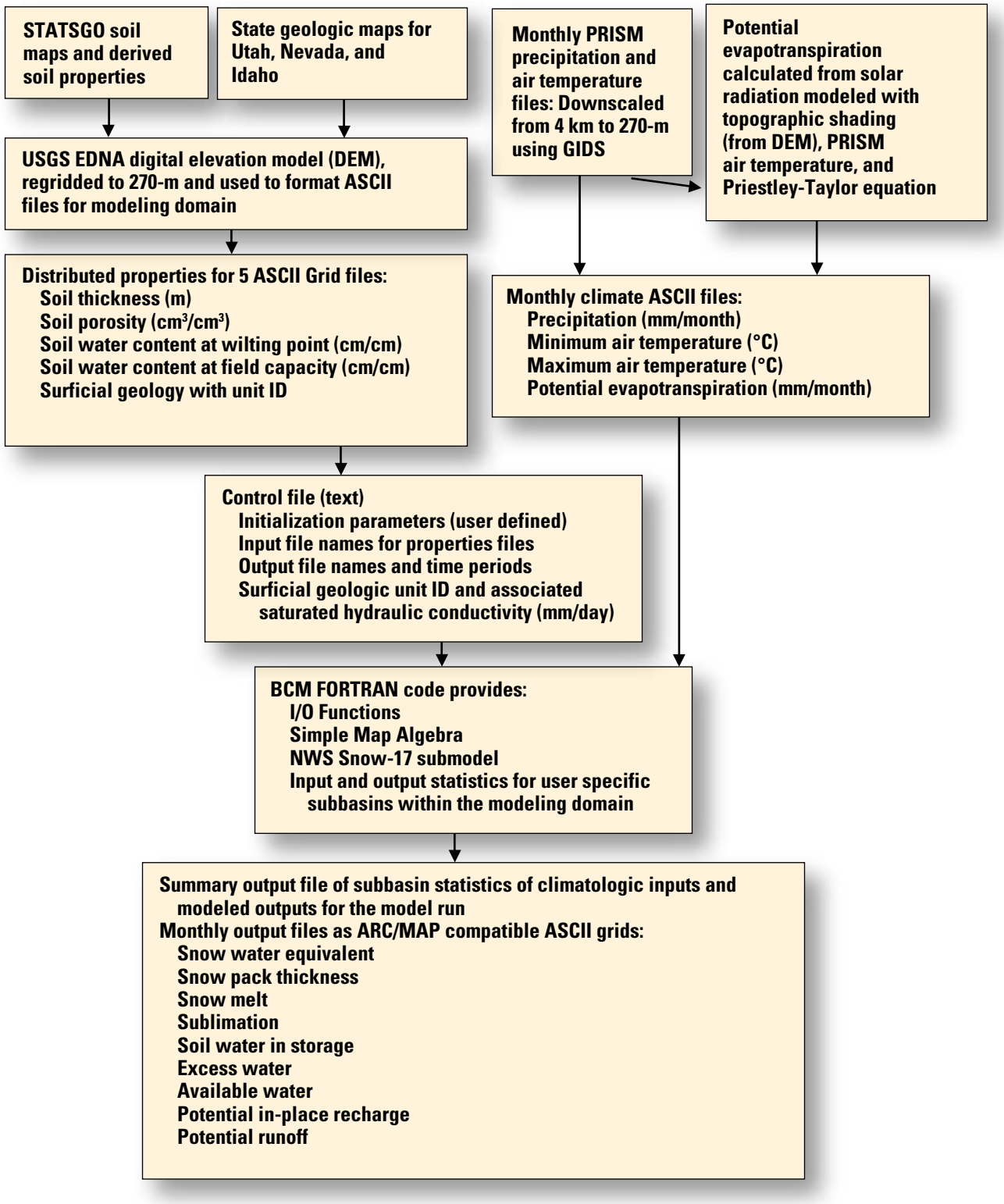

Definitions
BCM = Basin Characterization Model; DEM = Digital Elevation Model; EDNA = Elevation Derivatives for National Applications
GIDS = gradient plus inverse distance squared weighting; ID = identification; I/O = input/output; NWS = National Weather Service
PRISM = Parameter elevation Regressions on Independent Slopes Model; STATSGO = State Soil Geographic Database; m = meter; cm = centimeter; mm = millimeter; km = kilometer; °C = degrees Celsius

Figure A3–3. Input files required for operation of the Basin Characterization Model and optional output files resulting from simulations.

References Cited

Anderson, E.A., 1976, A point energy and mass balance model of a snow cover: Silver Spring, Maryland: National Oceanographic and Atmospheric Administration Technical Report NWS 19, 150 p.

Bedinger, M.S., Langer, W.H., and Reed, J.E., 1989, Groundwater hydrology, *in* Bedinger, M.S., Sargent, K.A., and Langer, W.H., eds., Studies of geology and hydrology in the Basin and Range Province, Southwestern United States, for isolation of high-level radioactive waste—Characterization of the Death Valley region, Nevada and California: U.S. Geological Survey Professional Paper 1370–F, p. 28–35.

Campbell, G.S., 1985, Soil physics with BASIC: Transport models for soil plant systems: Amsterdam, Elsevier, Developments in Soil Science, no. 14, 150 p.

Daly, C., Halbleib, M., Smith, J.I., Gibson, W.P., Doggett, M.K., Taylor, G.H., Curtis, J., and Pasteris, P.A., 2008, Physiographically-sensitive mapping of temperature and precipitation across the conterminous United States: International Journal of Climatology, vol. 28, no. 15, p. 2,031–2,064, doi: 10.1002/joc.1688, accessed Januray 20, 2009 at http://onlinelibrary.wiley.com/doi/10.1002/joc.1688/pdf.

Davis, S.N., and DeWiest, R.J.M., 1966, Hydrogeology: New York, John Wiley, 463 p.

Dettinger, M.D., Cayan, D.R., McCabe, G.J., and Marengo, J.A., 2000, Multiscale streamflow variability associated with El Niño/Southern Oscillation, *in* Diaz, H.F. and Markgraf, V., eds., El Niño and the Southern Oscillation, multiscale variability and global and regional impacts: Cambridge, Cambridge University Press, p. 113–147.

Flint, A.L., and Childs, S.W., 1987, Calculation of solar radiation in mountainous terrain: Journal of Agricultural and Forest Meteorology, v. 40, p. 233–249.

Flint, A.L., and Flint, L.E., 2007, Application of the basin characterization model to estimate in-place recharge and runoff potential in the Basin and Range carbonate-rock aquifer system, White Pine County, Nevada, and adjacent areas in Nevada and Utah: U.S. Geological Survey Scientific Investigations Report 2007–5099, 20 p.

Flint, A.L., Flint, L.E., Hevesi, J.A., and Blainey, J.M., 2004, Fundamental concepts of recharge in the Desert Southwest: a regional modeling perspective, *in* Hogan, J.F., Phillips, F.M., and Scanlon, B.R., eds., Groundwater recharge in a desert environment: The Southwestern United States: American Geophysical Union, Water Science and Applications Series, v. 9, p. 159–184.

Flint, A.L., Flint, L.E., Hevesi, J.A., D'Agnese, F.A., and Faunt, C.C., 2000, Estimation of regional recharge and travel time through the unsaturated zone in arid climates, *in* Faybishenko, B., Witherspoon, P., and Benson, S., eds., Dynamics of fluids in fractured rock: American Geophysical Union, Geophysical Monograph, v. 122, p. 115–128.

Flint, A.L., Flint, L.E., and Huntington, J.L., 2008, Regional evaluation of changes in potential evapotranspiration under a changing climate and influences on recharge and runoff, *in* International Conference on Computation Methods in Water Resources, 17th, July 2008, San Francisco, California, Proceedings.

Flint, L.E., and Flint, A.L., 1995, Shallow infiltration processes at Yucca Mountain—Neutron logging data 1984–93: U.S. Geological Survey Water-Resources Investigations Report 95–4035, 46 p.

Flint, L.E., and Flint, A.L., 2007, Estimation of hourly stream temperatures in unmeasured tributaries to the Lower Klamath River, California: Journal of Environmental Quality, v. 37, p. 57–68.

Freeze, R.A., and Cherry, J.A., 1979, Groundwater: Englewood Cliffs, New Jersey, Prentice-Hall, 604 p.

Glancy, P.A., 1986, Geohydrology of the basalt and unconsolidated sedimentary aquifers in the Fallon area, Churchill County, Nevada: U.S. Geological Survey Water Supply Paper 2263, 62 p.

Hintze, L.F., Willis, G.C., Laes, D., Sprinkel, D.A., and Brown, K.D., 2000, Digital geologic map of Utah: Utah Geological Survey Map 179DM, scale 1:500,000.

Iqbal, M., 1983, An introduction to solar radiation: Academic Press, 309 p.

Jennings, C.W., 1977, Geologic map of California: California Division of Mines and Geology Geologic Data Map no. 2, 1 sheet, scale 1:750,000.

Johnson, B.R., and Raines, G.L., 1996, Digital representation of the Idaho state geologic map, a contribution to the Interior Columbia Basin Ecosystem Management Project: U.S. Geological Survey Open-File Report 95–690, 24 p.

Lundquist, J.D., and Flint, A.L., 2006, 2004 onset of snowmelt and streamflow: How shading and the solar equinox may affect spring runoff timing in a warmer world: Journal of Hydrometeorology, v. 7, p. 1,199–1,217.

Nalder, I.A., and Wein, R.W., 1998, Spatial interpolation of climatic normals: Test of a new method in the Canadian boreal forest: Journal of Agricultural and Forest Meteorology, v. 92, no. 4, p. 211–225.

Priestley, C.H.B., and Taylor, R.J., 1972, On the assessment of surface heat flux and evaporation using large-scale parameters: Monthly Weather Review, v. 100, p. 81–92.

Shamir, E., and Georgakakos, K.P., 2005, Distributed snow accumulation and ablation modeling in the American River Basin: Advances in Water Resources, v. 29, no. 4, p. 558–570.

Shuttleworth, W.J., 1993, Evaporation, chap. 4 *of* Maidment, D.R. ed., Handbook of hydrology: New York, McGraw-Hill, p. 4.1–4.53.

Stewart, J.H., Carlson, J.E., Raines, G.L., Connors, K.A., Moyer, L.A., and Miller, R.J., 2003, Spatial digital database for the geologic map of Nevada: U.S. Geological Survey Open-File Report 03–66, version 3.0, 32 p.

Swinbank, W.C., 1963, Long-wave radiation from clear skies: Quarterly Journal of the Royal Meteorological Society, v. 89, p. 339–348.

Topp, G.C., and Ferre, P.A., 2002, Water content, *in* Dane, J.H., and Topp, G.C., eds., Methods of soil analysis, pt. 4, Physical methods: Soil Science Society of America Book Series 5, p. 417–419.

Soil Conservation Service, 1991, State soil geographic data base (STATSGO), data users guide: Washington, D.C., Soil Conservation Service, Miscellaneous Publication 1492, 88 p.

Winograd, I.J., and Thordarson, W., 1975, Hydrogeologic and hydrochemical framework, south-central Great Basin, Nevada-California, with special reference to the Nevada Test Site: U.S. Geological Survey Professional Paper 712–C, 126 p.